ACCOUNTING FOR THERMAL MASS IN THERMAL SIMULATION TOOLS: COMPARISON OF SEVERAL ASSUMPTIONS

Fabio Munaretto[1,2], Bruno Peuportier[1], Alain Guiavarch[1]
[1]MINES ParisTech - CES (Center for Energy efficiency of Systems), Paris, France
[2]CERIB (Studies and Research Center for the Precast Industries), Epernon, France

ABSTRACT

Being highly insulated, low energy buildings are very sensitive to variable solar and internal gains. In this context, thermal mass is useful in storing surplus energy, reducing temperature variations and improving thermal comfort. Thus, conduction modelling is fundamental, but not sufficient: appropriate superficial heat transfer modelling is also needed. Therefore, several common simplifying assumptions have been investigated and adapted to the case of high performance buildings. These models are reassessed using the BESTEST numerical building simulations and compared to reference models.

INTRODUCTION

Assessing energy, environmental and thermal comfort performances, depending on thermal mass among other factors, requires reliable building dynamic thermal simulation (DTS) tools. Historically, model developers have tried to find a fair-trade between accuracy and simulation efficiency within a fit-to-purpose philosophy [Lefebvre, 1987] [Ménézo et al., 2002]. Simplifying assumptions have therefore been integrated into DTS tools and is closely related to thermal mass. The validity of such assumptions, for instance constant internal convective and infrared radiative superficial exchange coefficients, or fixed distribution of solar gains transmitted through windows, has been proven for buildings with poor energy efficiency [EN ISO, 2008] but it particularly needs to be reassessed in the case of high performance buildings. For this reason, corresponding sophisticated models have been implemented into a simulation platform. A first step will involve simulations on a poorly energy-efficient simple enclosure case study: the IEA BESTEST [Judkoff and Neymark, 1995]. The influence of thermal mass on heating loads will be discussed using a simulation platform allowing several levels of model complexity to be implemented. Another publication will be dedicated to high performance buildings.

STANDARD SIMULATION PLATFORM

The simulation platform "StandardSP" used for this research is a reduced-order model based on finite volume method and modal analysis [Peuportier and Sommereux, 1990], which has been validated on poorly energy-efficient buildings [Peuportier, 2005].

Energy conservation equations

Energy conservation equations are expressed in [W] at all grid nodes centered in control volumes characterised by their respective heat capacities C [J/K], and homogenous temperatures. For instance, the zone node (including air and furniture, subscript $_z$) energy conservation equation represents equality between the variation of energy stored in the zone and the sum of advection, globalized convection and long-wave radiation (conv + lw. rad), conduction through opaque walls and windows including thermal bridges, short-wave radiation (sw. rad) and heating or cooling power (q_h) net heat fluxes:

$$C_z\dot{T}_z = q_{advection} + q_{thermal.bridges} + q_{sw.rad} + q_{conv+lw.rad+cond,windows+walls} + q_h \quad (1)$$

Net heat fluxes of interest are detailed below:

$$q_{sw.rad} = \sum_{i=1}^{N_{wall}} \frac{\alpha_i S_i}{\sum_{i=1}^{N_{wall}} \alpha_i S_i} \frac{\frac{R_{1,i}}{2}}{R_{g,i} + \frac{R_{1,i}}{2}} q_{sw.rad,z} \quad (2)$$

$$q_{conv+lw.rad+cond,walls} = \sum_{i=1}^{N_{wall}} \frac{1}{R_{g,i} + \frac{R_{1,i}}{2}} S_i\left(T_{1,i} - T_z\right) \quad (3)$$

Similar equations are outlined for each node, forming for each thermal zone a matrix equation: the state equation, linking the evolution of temperatures with temperature and driving force vectors (respectively T and Y). Another equation links the selected outputs (Y vector) with the same vectors: the output equation.

$$\begin{cases} C.\dot{T} = A.T + E.U \\ Y = J.T + G.U \end{cases} \quad (4)$$

This mathematical system is then reduced by eliminating short dynamics via a variable-change ($T = T_0 - A^{-1}.E.U$), a basis transformation (the mode vector $X = P^{-1}.T_0$ represents temperatures in the modal basis) and by sorting time constants. Ten modes are kept in the state equation (reduced model, subscript r), corresponding to a validated

compromise preserving the accuracy of outputs. These mathematical steps are known as the modal analysis [Bacot et al., 1984].

$$\begin{cases} \dot{X_r} = F_r.X_r + B_r.\dot{U} \\ Y = H_r.X_r + S.U \end{cases} \quad (5)$$

Zone coupling is then applied by using equivalent adjacent temperature in the Y_g vector instead of in the U vector (the distinction is made with B_g^{α}, B_g^{β}, ${S_g}^{\alpha}$ and ${S_g}^{\beta}$ matrix) and by gathering (subscript g) all zone matrices in one single global matrix [Blanc-Sommereux and Lefebvre, 1989].

$$\begin{cases} \dot{X_g} = F_g.X_g + {B_g}^{\alpha}.\dot{U_g} + {B_g}^{\beta}.\dot{Y_g} \\ Y_g = H_g.X_g + {S_g}^{\alpha}.U_g + {S_g}^{\beta}.Y_g \end{cases} \quad (6)$$

An integration on a Δt time step is also carried out:

$$\begin{cases} X_g^{n+1} = e^{\Delta t F_g}.X_g^n + W_g^{\alpha}.\left(U_g^{n+1} - U_g^n\right) \\ \qquad\qquad + W_g^{\beta}.\left(Y_g^{n+1} - Y_g^n\right) \\ Y_g^{n+1} = H_g.X_g^{n+1} + {S_g}^{\alpha}.U_g^{n+1} \\ \qquad\qquad + {S_g}^{\beta}.Y_g^{n+1} \end{cases} \quad (7)$$

The matrix equation system 7 can finally be solved by substituting X_g^{n+1} in the second equation by its expression in the first equation.

Simplifying assumptions

The simulation platform incorporates numerous simplifying assumptions. Among them, assumptions of interest for this research are:

- globalization of convective and long-wave radiative superficial heat transfer,
- constant convective and long-wave radiative transfer coefficients,
- wall area and short-wave absorptivity dependent distribution of solar gains.

An extended description of physical assumptions for buildings modelling with either low or high accuracy can be found in the literature [Clarke, 2001].

Global superficial transfer coefficients

As a simplifying assumption, convective and long-wave transfer coefficient, respectively h_{conv} and $h_{lw.rad}$ might be gathered in a global transfer coefficient h_g such as:

$$h_g = h_{conv} + h_{lw.rad} \quad (8)$$

Table 1 Internal convective transfer coefficients for different wall inclinations and flux directions.

Wall inclination	**Flux direction**	**Coefficient $h_{conv,int}$**
$[-]$	$[-]$	$[W/(m^2.K)]$
Vertical	Horizontal	3,29
Horizontal	Ascendant	4,59
	Descendant	1,78

Constant convective transfer coefficients

Main wall inclination and flux direction dependent internal convective transfer coefficients [Achard and Gicquel, 1986] are presented in Table 1.

Constant long-wave radiative transfer coefficients

Long-wave radiative heat transfer equations are linearized and temperatures with which the wall surface exchanges are assimilated to the zone temperature, where T_{ref}^3 is a reference temperature resulting from the linearization:

$$q_{lw.rad,i} \approx \varepsilon_i \sigma 4 T_{ref}^3 S_i \left(T_{s,i} - T_z\right) \quad (9)$$

Internal long-wave radiative transfer coefficients have been estimated, and whatever the type of wall i, $h_{lw.rad,i} = \varepsilon_i \sigma 4 T_{ref}^3$ is close to 4.84 W/(m².K) for an infrared emissivity ε_i equal to 0.9.

In the standard model, convective and long-wave superficial transfer coefficients are considered constant over the simulation period.

Transmission through windows and internal distribution of solar gains

The solar incident short-wave radiation density on a tilted window (w_i) surface is evaluated with a classic isotropic model [Duffie and Beckman, 1991], which splits global radiation into its direct ($_D$), diffuse ($_d$) and ground-reflected ($_r$) components:

$$q''_{sw.rad,w_i} = q''_{sw.rad,w_i,D} + q''_{sw.rad,w_i,d} + q''_{sw.rad,w_i,r} \quad (10)$$

The total solar gains transmitted through glazing (solar factor τ in terms of the angle of incidence), noted $q_{sw.rad,w}$, are then calculated:

$$q_{sw.rad,w} = \sum_{i=1}^{N_{glazing}} q''_{sw.rad,w_i} S_{w_i} \tau \quad (11)$$

A portion of $q_{sw.rad,w}$, depending on the average wall absorptivity ($\bar{\alpha}$), is first reflected on wall surfaces and transmitted back to the environment through the glazing. At the same time, a portion is reflected on internal glazing surfaces, then on wall surfaces and so on. These inter-reflexions within the zone are represented by an infinite geometric series such as $\sum_{n=0}^{\infty} r^n = 1/(1-r)$, where the common ratio r is defined as follows:

$$r = (1 - \bar{\alpha}) \left(1 - \bar{\tau} \frac{\sum_{i=1}^{N_{glazing}} S_{w_i}}{\sum_{i=1}^{N_{wall}} S_i - \overline{S_{wall}}}\right) \quad (12)$$

The fraction $F_{sw.rad,z}$ of $q_{sw.rad,w}$, remaining in a zone, corresponds to the flux $q_{sw.rad,z}$:

$$q_{sw.rad,z} = \bar{\alpha} * \frac{1}{1-r} q_{sw.rad,w} = F_{sw.rad,z}\, q_{sw.rad,w} \quad (13)$$

This short-wave energy flux is thereafter distributed to the walls proportionally to their absorptivity-area product ratio, and directed towards the first internal node of wall i proportionally to the thermal resistance

ratio between both sides of the wall surface ($R_{g,i}$ and $R_{1,i}/2$):

$$q_{sw.rad,1,i} = \frac{\alpha_i S_i}{\sum_{i=1}^{N_{wall}} \alpha_i S_i} \frac{R_{g,i}}{R_{g,i} + R_{1,i}/2} q_{sw.rad,z} \quad (14)$$

The part of $q_{sw.rad,z}$ that is not absorbed by opaque walls is finally allocated the zone node (cf. equation 2 which is equivalent) :

$$q_{sw.rad} = q_{sw.rad,z} - \sum_{i=1}^{N_{wall}} q_{sw.rad,1,i} \quad (15)$$

We have been through a brief introduction of the simulation platform exploited for this research. The simplifying assumptions of interest have been detailed. In the next section, a sophistication of these assumptions is carried out. In this way, the influence of thermal mass under a more realistic and reliable simulation environment is studied.

IMPROVED MODEL OF INTERNAL SUPERFICIAL HEAT TRANSFER

Decoupling internal convective and radiative heat transfers

Globalising convection and long-wave radiation phenomena leads to mix the air temperature T_{air} and the superficial wall and windows temperature $T_{s,i}$. Thus, the zone temperature T_z is close to an operative temperature, itself close to the average temperature between air and internal surfaces. Decoupling the two phenomena introduces a real T_{air} node and is essential to:

- improving physical reliability of each heat transfer,
- distributing heating power (q_h) either to air or walls surfaces depending on the heating system,
- using a thermostat sensing either air or operative temperature.

The Star model is a pseudo-decoupling model [Seem, 1987]. It has been preferred to decoupling models (e.g. recursive or radiosity methods) because of the complexity of making net long-wave radiation exchanges converge and the resulting time-consuming simulations. In the Star model, convective and radiative heat transfers are identified using thermal resistances as shown in Figure 1, presenting as well the global surface transfer coefficient model (noted "StandardSP" in this paper). The Star model introduces an air temperature that was not available in the standard simulation platform.

Thus, depending on the type of control and heating system, the heating power q_h (cf. equation 1) can be allocated either to the air, Star or first internal nodes of partitions with the desired proportions.

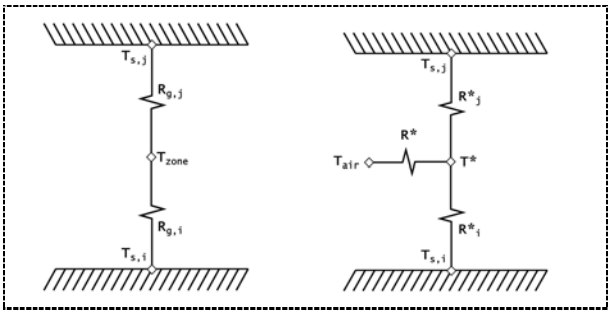

Figure 1 Global surface transfer coefficient model (left) and T^* model (right).

Internal long-wave radiation heat transfer

The expression of long-wave radiation thermal resistances in terms of wall surface temperatures rather than a reference temperature (T_{ref}) can be seen below:

$$R_{lw.rad,i-j} = \frac{1}{S_i Ge_{ij} \varepsilon_i \sigma 4 \left[\frac{(T_{s,i} + T_{s,j})}{2}\right]^3} \quad (16)$$

In addition, these thermal resistances can be re-assessed as frequently as it is necessary. It is noteworthy that the Gebhart matrix Ge needs a view-factor identification between each wall and window pair [Clark and Korybalski, 1974]. In this research, the view factors have been calculated manually for the case studies. We can imagine an approximating pre-process calculation in order to generalize the model [Aschaber et al., 2009].

Internal convection heat transfer

Several authors have tried to quantify internal surface convection exchanges and derive transfer coefficients.

Alamdari and Hammond made a great contribution with a set of correlations for buoyancy-driven convection (not valid for heaters). Alamdari and Hammond exploited pre-existing measurements realised on free-standing walls. Their correlations depend on the temperature difference between wall surface and air [Alamdari and Hammond, 1983]. Furthermore, geometric parameters are integrated in the equations.

Khalifa undertook his own experimental study in a test cell. As Alamdari and Hammond, he derived the convection coefficient from the energy balance equation at the tested wall surface [Khalifa and Marshall, 1990]:

$$h_{conv,i} = \frac{q_{lw.rad,net,i} + q_{cond,i}}{S_i(T_{air} - T_{s,i})} \quad (17)$$

He neglected the long-wave radiation exchanges by minimising the experimental net infrared radiation flux $q_{lw.rad,net,i}$. In addition, he measured the average surface temperatures at the front and behind the wall in order to quantify the conduction losses $q_{cond,i}$.

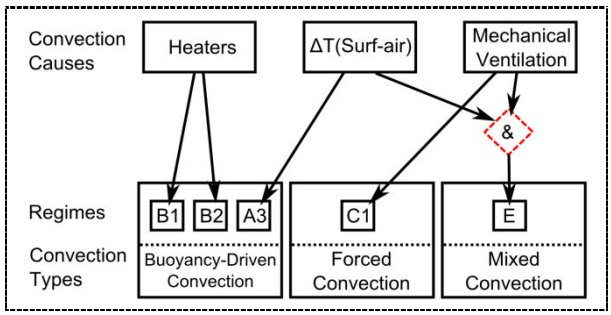

Figure 2 Partial representation of the internal convection formalism.

The air temperature was averaged as well. As $q_{lw.rad,net,i}$ was neglected (e.g. infrared exchanges with the heater), the criticisms were focused on the resulting coefficient over-estimation.

We introduced two major contributions. But a standard must be adopted in order to integrate all kinds of convection types and related correlations [Beausoleil-Morrison, 2000].

Thus, internal convective phenomenon might be described by:

- buoyancy-driven convection (Regimes A and B),
- forced convection (Regimes C and D),
- mixed convection (Regime E).

These convection regimes can be differentiated by their most common causes as it is represented in Figure 2.

Buoyancy-driven convection is due either to the temperature difference between air and walls, the presence of heaters or to heated wall panels, whereas forced convection is due to mechanical ventilation systems. Mixed convection is a combination of buoyancy-driven and forced convection.

Other correlations are available for forced (Air Change per Hour – ACH – dependent) and mixed convection (buoyancy-driven and forced convection correlation blending technique, ΔT and ACH dependent). They will not be described in this paper but have been studied nevertheless.

Again, as for internal infrared radiative heat transfer, the coefficients are assessed at each time step.

Distribution of solar gains

The simulation platform uses Test Reference Years weather-data files [Lund, 1985]. Solar radiation data includes global and diffuse solar irradiance on a horizontal plane, respectively $G_{g,h}$ and $G_{d,h}$. The direct component can be derived from these two values or included in the weather-data files if available for the selected site. The following sub-section explains the distribution of beam solar radiation transmitted through the glazing and absorbed by internal partitions.

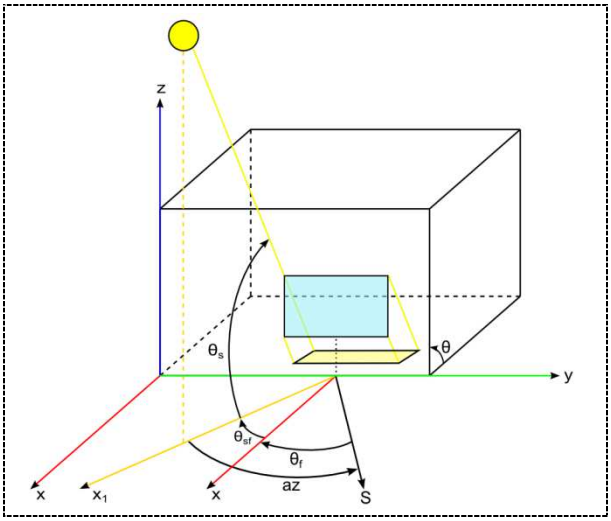

Figure 3 Geometric model of sun path tracking for a parallelepiped enclosure and a single glazing.

The other components (diffuse and reflected radiation) will be treated in a similar way as in equation 14 and 15.

A geometrical model tracking the sun path has been implemented in the simulation platform [Tittelein, 2008]. It calculates the area of projection of sunrays through a glazing on the different internal partitions of a parallelepiped enclosure.

The projection is first operated on two infinite planes: one containing the floor and another the wall facing the window. According to these projections, the model is able to discriminate the walls which are first reached by beam radiation. Then a geometrical calculation is carried out in order to evaluate the projected areas. Finally, the direct component, $q''_{sw.rad,w_i,D}$, of the global solar radiation density reaching the tilted wall, including the considered glazing, $q''_{sw.rad,w_i}$, is isolated (cf. equation 10).

Primary beam solar radiation transmitted through the glazing and absorbed at internal surfaces then needs to be evaluated on every partition. For nomenclature convenience, the wall including the window will be identified by the South direction and others by their related directions (see Figure 3). Therefore, beam solar radiation can strike either East (E), West (W), North (N) or Floor (F) partitions such as:

$$\begin{cases} q_{sw.rad,w_i,D,E} = \alpha_E S_E \tau q''_{sw.rad,w_i,D} \tan\theta_{sf} F_{sw.rad,z} \\ q_{sw.rad,w_i,D,W} = \alpha_W S_W \left(-\tau q''_{sw.rad,w_i,D} \tan\theta_{sf}\right) F_{sw.rad,z} \\ q_{sw.rad,w_i,D,N} = \alpha_N S_N \tau q''_{sw.rad,w_i,D} F_{sw.rad,z} \\ q_{sw.rad,w_i,D,F} = \alpha_F S_F \tau G_{D,h} F_{sw.rad,z} \end{cases} \quad (18)$$

The complementary part of the primary beam solar radiation reflected on internal surfaces after the sunray's first incidence is distributed proportionately to the absorptivity-area product to each internal surface and split as in the equations 14 and 15.

Correction of the linear reduced model

The modal analysis is intented to handle linear physical phenomena. However, non-linear phenomena or non-constant parts of the linear model can be managed after zone coupling and integration steps (see equation 7) by adding appropriate corrections in the U_g^{n+1} driving-force vector. For instance, if we consider the heat transfer between the Star and air nodes (see Star network in figure 1), giving the thermal resistance $R^*(t)$ expressed as $[K/W]$ which is a non-constant parameter, and the corresponding heat flux $\phi(t) = \frac{1}{R^*(t)}\left(T^*(t) - T_{air}(t)\right)$ expressed as $[W]$, then, the heat flux evaluated by the reduced modal model (subscript rmm) is $\phi_{rmm}(t) = \frac{1}{\overline{R^*}}\left(T^*(t) - T_{air}(t)\right)$. $\overline{R^*}$ is an averaged value initializing $R^*(t)$ which is placed in the A and E matrix of equation 4. $\phi_{rmm}(t)$ must be corrected in order to reflect the evolution of $R^*(t)$, such as $\phi(t) = \phi_{rmm}(t) + \Delta\phi(t)$. One can isolate the correction term $\Delta\phi(t)$:

$$\Delta\phi(t) = \left(\frac{1}{R^*(t)} - \frac{1}{\overline{R^*}}\right)\left(T^*(t) - T_{air}(t)\right) \qquad (19)$$

Afterwards, the correction heat flux $\Delta\phi(t)$ can be placed in the driving force vector U_g^{n+1} (see equation 7). Similar corrections are carried out for other time-dependent thermal resistances of the Star network. Concerning the distribution of solar gains within the zone, allocation either to first internal or air nodes is carried out at each time step with updated thermal resistances for each glazing.

An iterative process is carried out so that model outputs (temperatures, heating power) converge.

APPLICATION IN A CASE STUDY

The simulation platform is parametrised so that the user is able to choose the desired model sophistication level. Its basic level is represented by "StandardSP" (see model assumptions in the

Standard simulation platform section). The next level of the model complexity integrates the Star model (i.e. pseudo-decoupling internal long-wave radiative and convective transfer) with more accurate, and updated at each time step, internal long-wave radiation transfer between all internal surfaces: "T*SP". Increasing the level of sophistication of convection algorithm within the "T*SP" frame will lead to the "T*ConvSP" model. Finally, introducing the sun path tracking model will generate the last level of complexity: "T*ConvSunSP".

Case study: IEA BESTEST

A world-wide recognised study has been chosen for its simplicity, precise description and benchmark philosophy : the International Energy Agency Building Energy Simulation TEST (BESTEST) and Diagnostic Method [Judkoff and Neymark, 1995]. Its basic geometry is described in Figure 4.

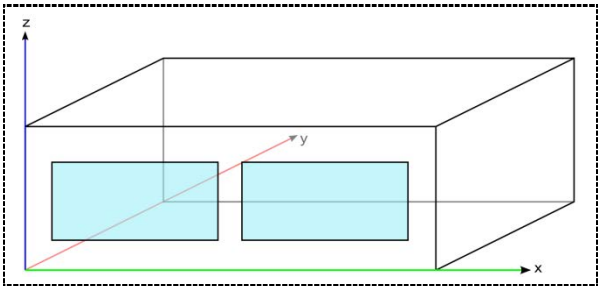

Figure 4 Simple parallelepiped enclosure with two windows (BESTEST basic geometric description).

A certain number of test cases have been chosen to evaluate the influence of thermal mass under different levels of model sophistification:

Table 2 Description of the BESTEST case studies

Case N°	Thermal Mass	Glazing Orientation	Night Setback
600	Low	South	No
900	High	South	No
620	Low	East/West	No
920	High	East/West	No
640	Low	South	Yes
940	High	South	Yes

Additional free-floating test cases 600FF and 900FF have been studied. Besides, the T*ConvSunSP model is not able to evaluate the solar gains of cases 620 or 920 due to windows included in two facing walls (East and West).

Simulation results

The BESTEST specifies that the heating device is a 100% convective air heating system (100% of heating power q_h is allocated to the air node), with a nonproportional-type thermostat sensing only the air temperature. Annual heating loads have been evaluated within the simulation platform. These results can be compared with recognised dynamic thermal simulation software such as TRNSYS 17.1[1], ESP-r 11.10[2] and EnergyPlus 7.2[3] in Figure 5. Operative temperatures of free-floating test cases 600FF and 900FF for StandardSP and the most sophisticated implemented model T*ConvSunSP during one sunny winter's day can be observed in Figure 6.

[1] ASHRAE Standard 140-2007, results for TRNSYS 17.01.0016 prepared by TRANSSOLAR

[2] Results available in ESP-r last available version.

[3] ANSI/ASHRAE Standard 140-2011, results for EnergyPlus 7.2.0.006 prepared by the U.S. DoE

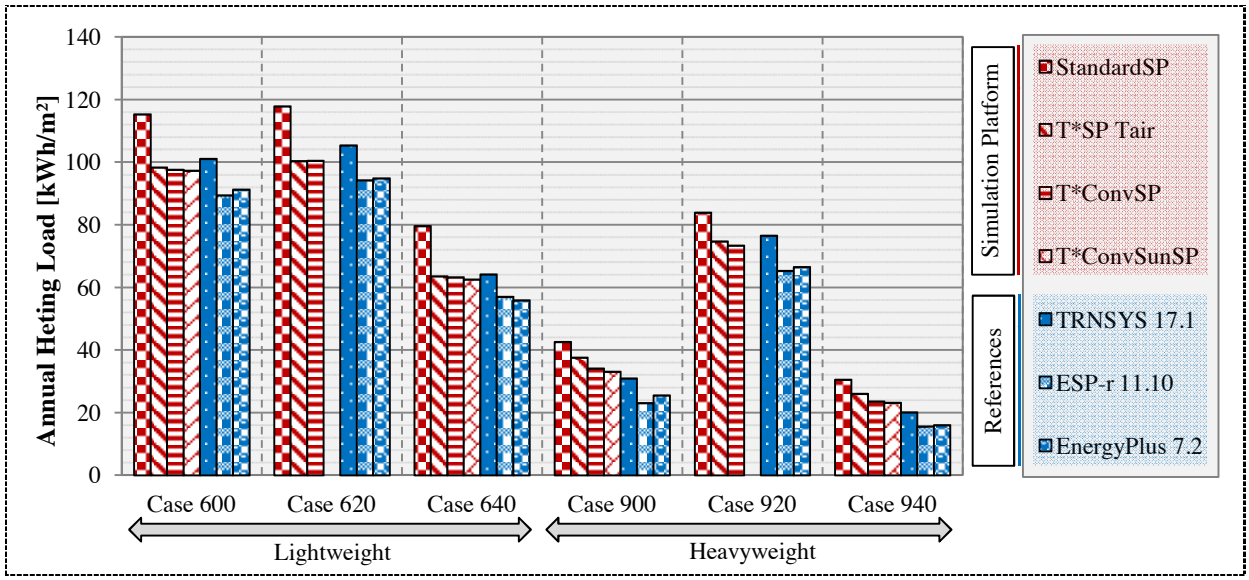

*Figure 5 Annual heating load per unit area of floor, of test cases 600, 620, 640, 900, 920 and 940 for StandardSP, T*SP, T*ConvSP, T*ConvSunSP, TRNSYS 17.1, ESP-r 11.10 and EnergyPlus 7.2 models.*

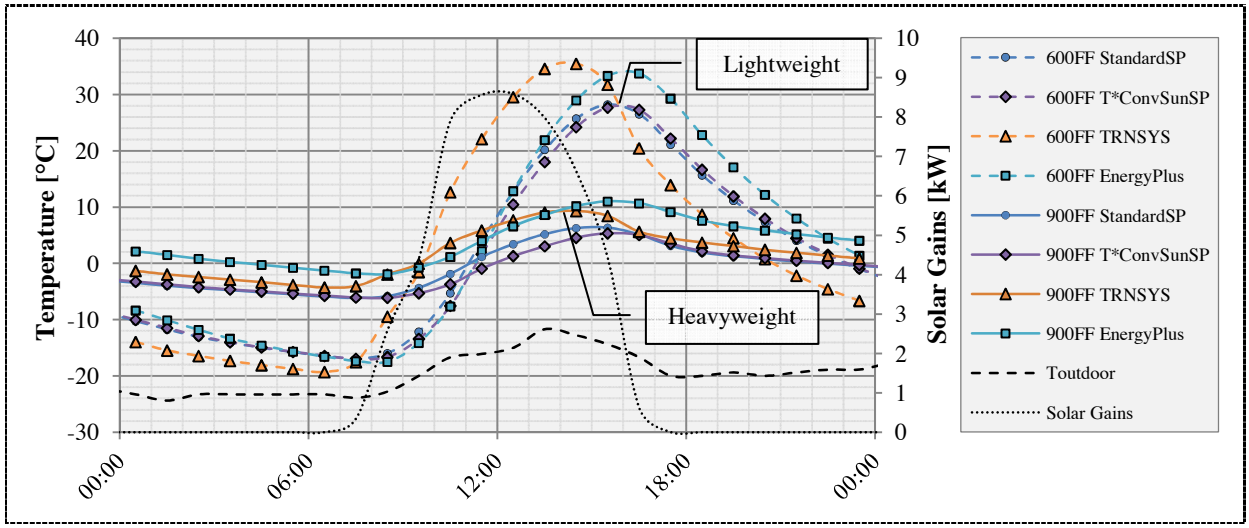

*Figure 6 Fourth of January outdoor temperature, solar gains and operative temperature curves of free-floating test cases 600FF and 900FF for StandardSP, T*ConvSunSP, TRNSYS 16 and EnergyPlus v6 models.*

The thermal mass effect

Cases 600 and 900 have different global heat capacities ($C_{600} = 596\ 617\ J/K$; $C_{900} = 4\ 536\ 878\ J/K$). Thanks to high thermal mass and high solar gains, the annual heating loads of case 900 are divided by three compared to those of lightweight case 600 (see Figure 5).

Besides, as a bioclimatic design parameter, orientation of windows strongly interacts with thermal mass. Moving from East/West to a southerly orientation reduces by half the heating load of the heavyweight case (-52% in average on all models from case 920 to 900) while it has much less influence in the lightweight case (-4,6% from case 620 to 920) as can be seen in Figure 5. However, benefits from a lower temperature setpoint during the night period (10°C) are similar between heavyweight and lightweight cases (-35% in average).

Influence of control temperature

The standard simulation platform including simplifying assumptions leads to an over-estimation of annual heating loads (between +10/25% and +20/70% respectively compared to implemented models and average reference models, see Figure 5). This result is mainly due to convection and long-wave radiation globalization. Indeed, zone temperature corresponds to an operative temperature. The thermostat senses this temperature and heating power is allocated completely to the related node. Therefore, much more energy is required to maintain air as well as surface temperatures close to the setpoint temperature. But this may correspond to a realistic behaviour: even if the thermostat is sensing the air temperature, the occupants' feeling is rather related to the operative temperature. Indeed, if the air is warm but the wall surfaces are cold, occupants will

increase the thermostat setpoint. The standard model might therefore be a better approximation of the heating load as it is in real life.

Additionally, standard and advanced models have been compared with an equivalent control temperature (zone temperature and operative temperature respectively for StandardSP and implemented advanced models). Still, the standard simulation platform leads to over-estimated annual energy requirements (between +1% and +6% compared to implemented models).

Influence of implemented models

As shown in Figure 5, the more the implemented models' complexity increases, the more their heating loads are close to those of the averaged reference models. This means that sophisticating internal heat transfer models contributes to the improvement of the reliability of the simulation platform with a limited increase of computation time efforts (3.1, 5.5, 5.9 and 6.1 seconds respectively for StandardSP, T*SP, T*ConvSP and T*ConvSunSP models - case 600 with a yearly period using a 30 minute time step). Moreover, the gain in precision is greater for a high thermal-mass, which corresponds to a better thermal performance. This result has a physical consistency because superficial heat transfer has a larger impact if superficial layers have the ability to store energy.

Additionally, Figure 6 shows that the dynamic behaviour of improved simulation platform temperature curves is closer to reference ones. Still, it appears that a discrepancy remains, which is probably related to heat loss issues.

The improved distribution of beam solar radiation induced by the geometric model of sun path tracking (see Figure 3), is not playing a fundamental role. Besides, the single introduction of the Star model without the improved convection algorithm seems to be inconsistent because long-wave radiation heat transfer coefficients are evaluated at each time step while convection coefficients are considered as constant. Thus, R* (see Figure 1) variability is very low and cannot modulate the heat transfer to the air node. Therefore, the modeller should associate the pseudo-decoupling Star model with time-dependent convection and long-wave radiation heat transfer coefficients.

Finally, we studied the interaction between model complexity and the number of modes (equation 4). The number of modes kept in the reduced model may influence the evaluated benefit of thermal mass, i.e. the difference between annual heating load of cases 600 and 900: $\Delta AHL_{N_{Modes}} = AHL_{600,N_{Modes}} - AHL_{900,N_{Modes}}$, number of modes N_{Modes} ranging between 1 and 24 (unreduced model). Then, we derived an indicator representing the error due to the model reduction $Err(N_{modes}) = (\Delta AHL_{N_{Modes}} - \Delta AHL_{24_{Modes}})/\Delta AHL_{24_{Modes}}$.

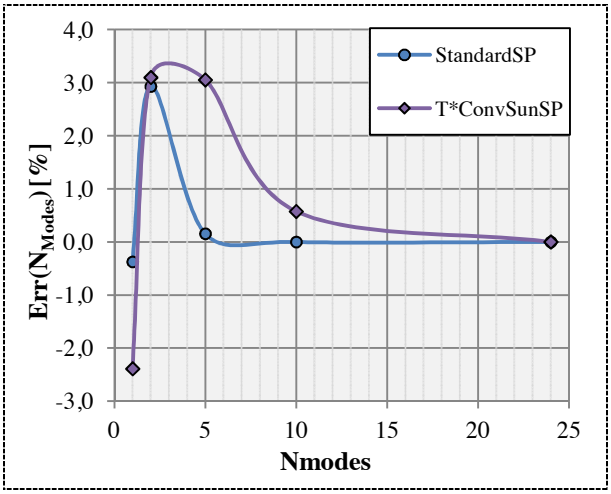

*Figure 7 Difference of annual heating load (between light and heavyweight cases of models StandardSP and T*ConvSunSP) error due to the model reduction.*

Figure 7 shows that the most complex model implemented (T*ConvSunSP) requires more modes to minimize the error done on the difference of annual heating load between light and heavyweight cases but 10 modes (number of modes used in the standard simulation platform) is still a good compromise. Similar results have been found concerning indicators quantifying the peaks of operative temperatures in summer.

Research limitations

Comparing different conduction models has not been addressed in this communication. Basic simulations increasing the number of nodes in wall partitions and reducing first internal layer thickness have been carried out, yet without a major influence. Also, interaction between implemented models is difficult to assess but should be considered more deeply, as well as the causes of model discrepancy: there is more difference between TRNSYS and EnergyPlus than between the different models compared on the same simulation platform (see Figure 6).

CONCLUSION

In the context of low energy buildings, thermal-mass effects are mainly due to a succession of heat storage and release stages (variable solar and internal gains) in the superficial internal layers of wall partitions.

Thus, we focused on related heat transfer modelling. We questionned some assumptions regarding convection, long-wave radiation and the distribution of solar gains, and compared their associated models, which were implemented in the same simulation platform so that the analysed discrepancies are only due to the compared assumptions. As a first step, an internationally recognised case study with poor performance buildings was used. Within this framework, annual heating load results suggest that:

- sophisticated implemented models are closer to reference models,

- type of setpoint temperature has a large influence,
- discrepancies are larger with heavyweight test cases,
- improved modelling of beam solar radiation distribution has little influence,
- ten modes seem appropriate in a reduced model.

These conclusions will be reassessed in a future research concerning a low-energy experimental case study (passive houses).

NOMENCLATURE

$T_{1,i}$: temperature of wall i first internal node [°C]
T_z: zone temperature [°C]
α: short-wave radiation absorptivity $[-]$
S: area $[m^2]$
$R_{1,i}$: thermal resistance of wall i first internal volume control $[m^2.K.W^{-1}]$
$R_{g,i}$: global superficial thermal resistance of wall i $[m^2.K.W^{-1}]$
$q_{sw.rad,z}$: solar gains remaining in a zone [W]

ACKNOWLEDGMENT

Collecting BESTEST results for reference models would not have been possible without exchanging with Marion Hiller (TRANSSOLAR for TRNSYS 17.1) and Paul Strachan (University of Strathclyde for ESP-r 11.10). The authors gratefully acknowledge the Studies and Research Center for the Precast Industries (CERIB, Epernon) for its support.

REFERENCES

Achard, P., and Gicquel, R. (1986). European passive solar handbook (Bruxelles: Commission of the european communities).

Alamdari, F., and Hammond, G.P. (1983). Improved data correlations for buoyancy-driven convection in rooms. Building Services Engineering Research and Technology *4*, 106–112.

Aschaber, J., Hiller, M., Weber, R., and Gmbh, T.E. (2009). TRNSYS17: New features of the multizone building model. In Eleventh International IBPSA Conference, (Scotland).

Bacot, P., Neveu, A., and Sicard, J. (1984). Analyse modale des phénomènes thermiques en régime variable dans le bâtiment. Revue générale de thermique *23*, 189–201.

Beausoleil-Morrison, I. (2000). The adaptive coupling of heat and air flow modelling within dynamic whole-building simulation. Doctorate Thesis. University of Strathclyde.

Blanc-Sommereux, I., and Lefebvre, G. (1989). Simulation de bâtiments multizones par couplage de modèles modaux réduits. Chauffage, ventilation, conditionnement *65*, 31–37.

Clark, J.A., and Korybalski, M.E. (1974). Algebraic methods for the calculation of radiation exchange in an enclosure. Wärme- Und Stoffübertragung *7*, 31–44.

Clarke, J.A. (2001). Energy simulation in building design (Butterworth-Heinemann).

Clarke, J.A., and Yaneske, P.P. (2009). A rational approach to the harmonisation of the thermal properties of building materials. Building and Environment *44*, 2046–2055.

Duffie, J.A., and Beckman, W.A. (1991). Solar engineering of thermal processes (Wiley).

EN ISO (2008). EN ISO 13790: 2008 Energy performance of buildings-Calculation of energy use for space heating and cooling.

Judkoff, R., and Neymark, J. (1995). International Energy Agency Building Energy Simulation Test (BESTEST) and Diagnostic Method (Golden, CO: National Renewable Energy Laboratory).

Khalifa, A.J.N., and Marshall, R.H. (1990). Validation of heat transfer coefficients on interior building surfaces using a real-sized indoor test cell. International Journal of Heat and Mass Transfer *33*, 2219–2236.

Lefebvre, G. (1987). Analyse et réduction modales d'un modèle de comportement thermique de bâtiment. Doctorate Thesis, University Paris VI.

Lund, H. (1985). Short reference years and test reference years for EEC countries: Final report (Technical University of Denmark).

Ménézo, C., Roux, J.J., and Virgone, J. (2002). Modelling heat transfers in building by coupling reduced-order models. Building and Environment *37*, 133–144.

Peuportier, B. (2005). Bancs d'essais de logiciels de simulation thermique. (Ecole Nationale Supérieure des Mines de Paris).

Peuportier, B., and Sommereux, I.B. (1990). Simulation tool with its expert interface for the thermal design of multizone buildings. Int. J. of Sustainable Energy *8*, 109–120.

Seem, J.E. (1987). Modelling of Heat Transfer in Buildings. Doctorate Thesis. University of Wisconsin.

Tittelein, P. (2008). Environnements de simulation adaptés à l'étude du comportement énergétique des bâtiments basse consommation. Doctorate Thesis. University of Savoie.